Available online at www.sciencedirect.com
SCIENCE DIRECT®
International Journal of Heat and Fluid Flow 24 (2003) 334–344
International Journal of HEAT AND FLUID FLOW
www.elsevier.com/locate/ijhff

Hydrodynamic and statistical parameters of slug flow

Lev Shemer *

Department of Fluid Mechanics and Heat Transfer, Faculty of Engineering, Tel-Aviv University, Tel-Aviv 69978, Israel

Abstract

In two-phase slug flow pattern, the bulk of the gas is trapped inside large bubbles that are separated by liquid slugs, which may contain small dispersed bubbles. The unsteady nature of slug flow makes the prediction of pressure drop and heat and mass transfer a difficult task. Earlier models that deal with steady slug flow assume constant lengths and shapes of liquid slugs and elongated bubbles, as well as a constant elongated bubble propagation velocity. However, due to the intrinsically irregular character of slug flow, statistical means are required for its proper description. Variation of the flow parameters along the pipes of various diameters and inclinations may strongly affect the resulting flow pattern and should thus be taken into account in modeling the flow. The development of slug flow along the pipe is mainly governed by the interaction between consecutive elongated bubbles. To gain a better insight into the mechanisms that govern slug flow evolution along pipes, experiments with controlled injection of consecutive elongated bubbles were performed in recent years. Due to the complexity of both the continuous slug flow and the liquid flow around injected bubbles, sophisticated experimental methods are required. The latest works regarding the hydrodynamic and statistics of naturally occurring continuous slug flow in pipes, as well as the results of experiments with controlled injection of elongated bubbles are reviewed. It is demonstrated how the information obtained in the controlled experiments can be applied to improve the performance of slug flow and slug tracking models.

Keywords: Two-phase pipe flow; Slug flow; Taylor bubble; Translational velocity

1. Introduction

Gas–liquid slug flow is one of the most complex flow patterns and is intrinsically unsteady. It often occurs e.g. in transportation of oil–gas mixtures in pipes from wells to the reservoirs. The prediction of pressure drop and gas–liquid spatial distribution within the pipeline is of utmost importance and requires proper knowledge of the relevant hydrodynamic parameters. It is generally assumed that the movement of the trailing bubble is affected by the velocity field in the liquid phase ahead of it. Information on the mean and instantaneous velocity fields around elongated bubbles, as well as the local instantaneous void fraction distribution within the liquid slug, are therefore indispensable for the understanding the relative movement of elongated and dispersed gas bubbles in pipelines of various inclinations.

In vertical slug flow most of the gas is located in large bullet-shaped bubbles (Taylor bubbles) that span most of the pipe cross-section. The liquid slugs that separate the elongated bubbles may be aerated with small gas bubbles. The liquid confined between the Taylor bubbles and the pipe wall flows around the bubble as a thin film. On the average, vertical slug flow retains axial symmetry. The flow regime in the liquid phase is often turbulent. Instantaneous (as opposed to the average) distributions of the velocity components, as well as of the void fraction, lack the axial symmetry. For vertical flow, both elongated bubble nose and tail exhibit strong oscillations (Polonsky et al., 1999a; Aladjem Talvy et al., 2000). The complex character of the flow around the Taylor bubble nose is demonstrated in Fig. 1, where consecutive snapshots of the distorted elongated bubble nose interfaces are shown. It can be clearly seen that the elongated bubble shape is varying constantly and the bubble nose sways from one side to the other. Most dispersed bubbles in the liquid slug are consumed by the elongated bubbles, but some of them penetrate into the liquid film. At pipe inclinations different from vertical even the symmetry on the average is lacking, and the

* Tel.: +972-3-640-8128; fax: +972-3-640-7334.
E-mail address: shemer@eng.tau.ac.il (L. Shemer).

0142-727X/03/$ - see front matter © 2003 Elsevier Science Inc. All rights reserved.
doi:10.1016/S0142-727X(03)00024-9

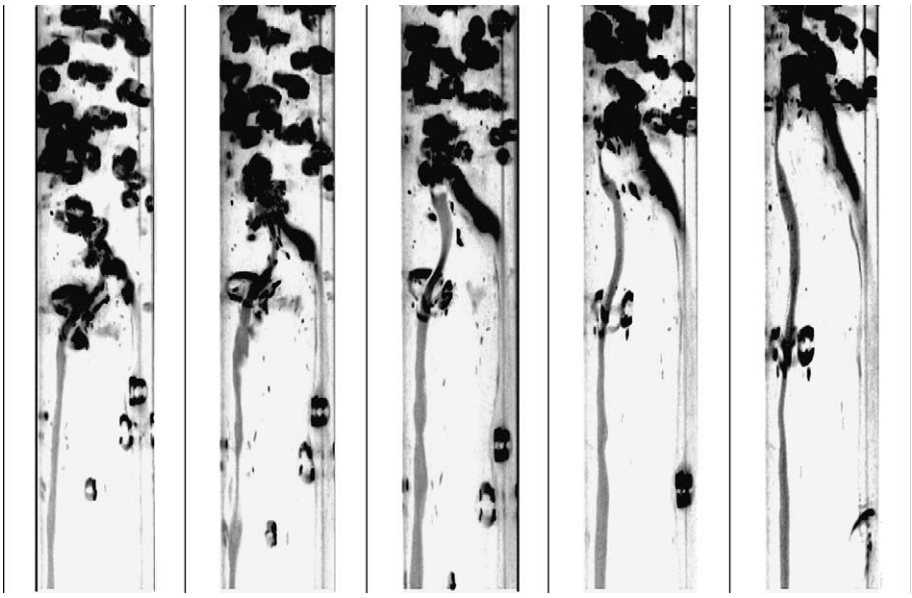

Fig. 1. Series of images of a swaying bubble nose in a continuous slug flow. $D = 0.024$ m, time interval between frames $\Delta t = 0.017$ s.

liquid slugs that fill the whole cross-section of the pipe are separated by stratified zones with elongated bubbles in the upper part of the pipe.

The high velocities in the liquid film region of slug flow and the strong mixing in the elongated bubble wake cause substantial enhancement of heat transfer. In some circumstances the measured heat transfer coefficients in slug flow can become comparable to those observed during condensation of pure vapors (Shoham et al., 1982). The quantitative data on the heat transfer characteristics in slug flow are, however, very limited at present. In part this results from considerable difficulties in conducting accurate and detailed experiments in both spatially and temporally randomly varying conditions. The lack of detailed understanding of hydrodynamics of slug flow also prevents sufficiently accurate modeling that could provide required data. Complete description of slug flow hydrodynamics apparently includes the mean flow parameters, such as characteristic velocities of propagation of liquid–gas interfaces, the characteristic lengths and shapes of elongated bubbles and liquid slugs, the distribution of the shear stresses along the slug unit and the spatial distribution of the void fraction in the liquid slug. The knowledge of the mean values is, however, insufficient for truthful modeling, and the data are also required on the range of variation of the instantaneous slug flow parameters and their statistical moments. Of particular importance is the maximum possible slug length since slug catchers design in the petroleum industry depends on the longest encountered slug. Moreover, transients are rather frequent and the development of the liquid slug and Taylor bubble length distributions from undeveloped to developed slug flow should be considered. The first part of this paper deals with some recent works on the statistics of developing slug flow. The complexity of continuous slug flow, however, suggests that a better insight into the underlying physical mechanisms can be gained if a simpler system, consisting of either a single or a short sequence of elongated bubbles moving in a pipe, is analyzed in greater detail. The second part of this paper presents recent progress in this direction and the implication of these studies on slug flow modeling.

2. Continuous slug flow

The evolution of slug flow along a pipeline strongly depends on the relative velocities between the elongated bubbles. At short separations, trailing elongated bubbles accelerate and eventually merge with the leading ones (Moissis and Griffith, 1962; Pinto et al., 1998; Aladjem Talvy et al., 2000). During the merging process, both the liquid slug and the elongated bubble lengths increase. This process is assumed to terminate once the liquid velocity profiles at the back of the liquid slug are fully developed and all elongated bubbles propagate at the same translational velocity. Nicklin et al. (1962) proposed a correlation for the calculation of the translational; velocity of an elongated bubble in continuous slug flow:

$$U_{\mathrm{Nick}} = CU_{\mathrm{m}} + U_{\mathrm{d}}, \tag{1}$$

where U_{d} is the drift velocity of the bubble in a stagnant liquid, and U_{m} is the mixture velocity defined as the sum of the liquid and gas superficial velocities, U_{LS} and U_{GS} The value of the constant C is based upon the assumption that the propagation velocity of the bubbles follows

the maximum local velocity, U_{max} in front of the nose tip and thus $C = U_{max}/U_m$ (Nicklin et al., 1962; Bendiksen, 1984; Shemer and Barnea, 1987; Polonsky et al., 1999b). The value of C therefore equals approximately 1.2 for fully developed turbulent flow and 2.0 for fully developed laminar flow.

The drift velocity U_d depends on the inclination angle β, and has a maximum for $40 < \beta < 60°$ (Zukoski, 1966; Bendiksen, 1984; Fabre and Liné, 1992; van Hout et al., 2002b). Furthermore, U_d increases with decreasing surface tension parameter $\Sigma = 4\sigma/\Delta\rho\, gD^2$ (Zukoski, 1966), where g is the gravitational constant, D the pipe diameter, σ the surface tension and $\Delta\rho$ the density difference between the liquid and the gas phases. For inclined flows, U_d has been correlated by Bendiksen (1984) as a weighted superposition of the drift velocity in a vertical pipe, U_d^v , and in a horizontal pipe, U_d^h:

$$U_d(\Sigma, \beta) = U_d^h(\Sigma, \alpha_B)\cos\beta + U_d^v(\Sigma, \alpha_B)\sin\beta, \qquad (2)$$

where α_B is the void fraction in the film region of the elongated bubble. Limiting values of U_d for negligible Σ (<0.001) were determined by Dumitrescu (1943) for the vertical case, $U_d^v = 0.35\sqrt{gD}$, and by Benjamin (1968) for the horizontal case, $U_d^h = 0.54\sqrt{gD}$.

Most experimental research concerning length distributions has been focused on determining the mean and maximum liquid slug lengths. Mean liquid slug lengths $\langle \ell_s \rangle$ (measured in D) were found to be relatively independent of flow rates. Measured normalized mean liquid slug lengths for vertical flow lie in the range from 10 to 20 with standard deviations between 30% and 50% (Griffith and Wallis, 1961; Barnea and Shemer, 1989; van Hout et al., 1992, 2001; Nydal et al., 1992; Costigan and Whalley, 1997). Felizola and Shoham (1995) found for inclined air–kerosene slug flow that $\langle \ell_s \rangle$, averaged over all investigated flow rates, has a minimum of about $16D$ at $\beta = 60°$. For the horizontal case, reported mean liquid slug lengths vary between 10 and $100D$ (Nydal et al., 1992; Andreussi et al., 1993). Maximum lengths have been reported to be 2–3 times the mean lengths.

Experimental measurements of the liquid slug and elongated bubble length distributions have been carried out mainly for horizontal or slightly inclined slug flow and for vertical flow. The liquid slug length distribution can be described by positively skewed distributions, such as the log-normal, the gamma, or the inverse Gaussian (Dhulesia et al., 1991; Nydal et al., 1992; van Hout et al., 2001). Modeling of the evolution of slug flow was undertaken by Bernicot and Drouffe (1989) for the horizontal case and by Barnea and Taitel (1993) for all inclination angles. The latter model was verified against experimental data for the slightly inclined case by Cook and Behnia (2001) and for the vertical case by van Hout et al. (2001). Model predictions compared reasonably well with the experimental data. The dependence of the elongated bubble translational velocity on the liquid slug length ahead of it, $U_t = f(\ell_s)$, should be provided as an input relation to the Barnea and Taitel model.

Our recent experimental results on the evolution of various hydrodynamic and statistical parameters of slug flow along inclined pipes are presented in the rest of this section. In particular, the relation of the instantaneous elongated bubble nose velocity to the liquid slug length ahead of it was measured. This is essential for developing reliable models for the prediction of the evolution of slug length distributions.

2.1. Experimental facility and procedure

The experimental facility consists of two 10 m long, parallel transparent Perspex pipes which have internal diameters of 0.024 and 0.054 m. Only results for $D = 0.024$ m are presented here. The system can be rotated around its axis and fixed at any inclination angle from horizontal to vertical. Measurements in upward inclined co-current slug flow were carried out using optical fiber probes that detect the local instantaneous phase at their tip (i.e. gas or liquid). Three probes with spacing of 0.02 m were mounted on a measurement module. The evolution of slug flow along the pipe was measured by placing the module at different positions x/D along the pipe, where the axial coordinate x is measured from the inlet.

Instantaneous propagation velocities, U_{inst} of each elongated bubble nose or tail interface were determined by the time interval required for the interface to move from one probe to the other. The elongated bubble lengths were calculated by multiplying the residence time of the gas bubble over the probe tip by the bubble nose velocity. The liquid slug lengths ahead of the bubble were then found by multiplying the residence time of the liquid slug by the instantaneous velocity of the preceding elongated bubble tail. Thus, the relation between the instantaneous elongated bubble velocity and the liquid slug length in front of it, $U_{inst} = f(\ell_s)$, as well as characteristic translational velocities at different measurement positions and inclination angles were determined. More details on the experimental facility and data processing can be found in van Hout et al. (2001, 2003).

2.2. Experimental results on the evolution of slug flow along inclined pipes

Measurements were carried out for different flow rates at various inclination angles. Typical ensemble-averaged results on instantaneous translational velocities of a trailing bubble nose as a function of the separation distance, $\langle U_{inst} \rangle = f(\ell_s)$, are presented in Fig. 2 at different locations along the pipe for $U_{LS} = 0.01$ m/s, $U_{GS} = 0.41$ m/s. The corresponding liquid slug length distributions are also shown. The bin size in the histo-

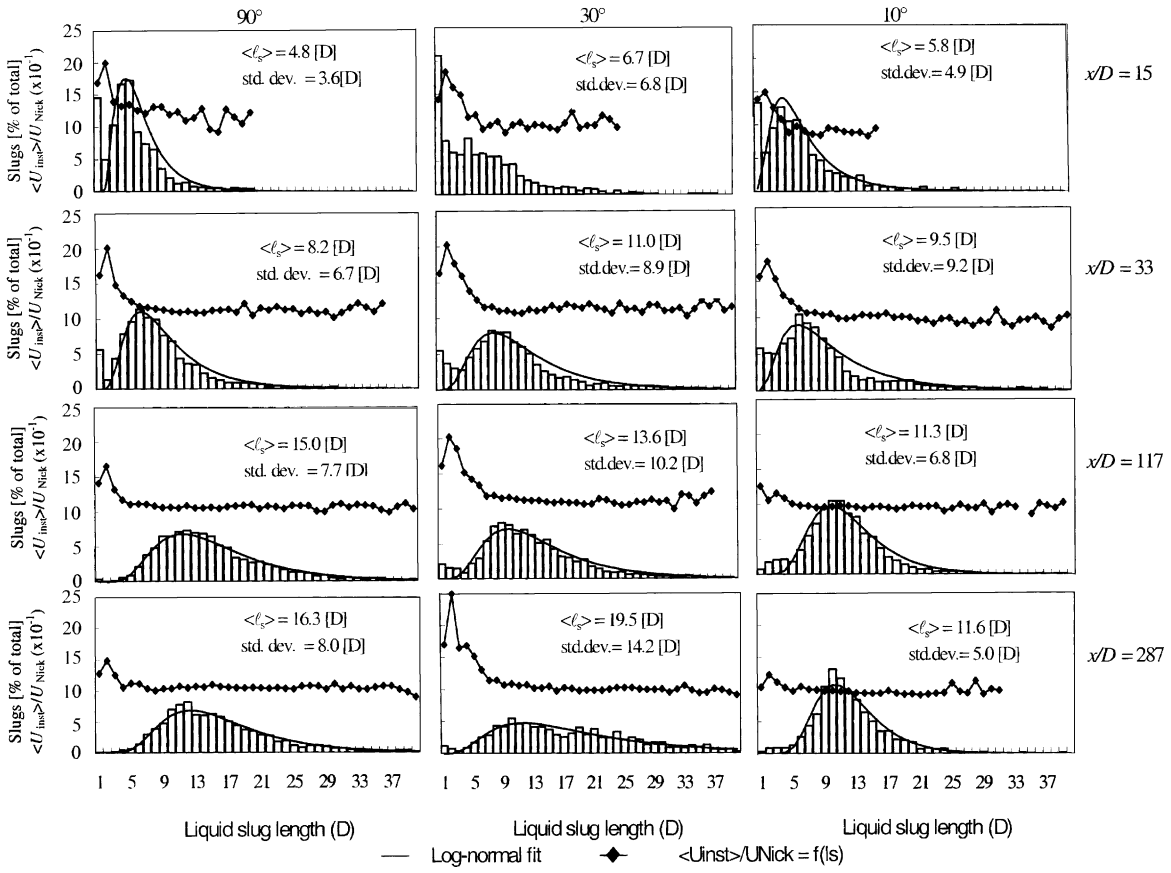

Fig. 2. Instantaneous translational velocity as a function of separation distance and the liquid slug length distribution based on the instantaneous velocity at various positions along the pipe (for three inclination angles relative to horizontal $U_{LS} = 0.01$ m/s; $U_{GS} = 0.41$ m/s).

grams is the pipe diameter D. For each bin separately, the corresponding trailing bubble velocities were averaged, yielding the ensemble-averaged value $\langle U_{inst} \rangle$. The standard deviations range between 10% and 50%. The instantaneous velocities are in general characterized by higher values at small separation distances and a constant lower propagation velocity at increasing values of ℓ_s. At $\ell_s < D$, just prior to coalescence, both bubbles travel at approximately the same velocity which causes a drop in the approach velocity. Velocities at large separation distances are well predicted by (1). The evolution of the measured liquid slug length distribution is also shown in Fig. 2. The mean and the mode of the length distributions, as well as the standard deviation, increase along the pipe. Both the liquid slug and the elongated bubble length distributions are right-skewed (tails extending to large values). The log-normal shape (solid line) was fitted to the measured distributions.

The accumulated data on $\langle U_{inst} \rangle / U_{Nick}$ where U_{Nick} is defined by (1), as a function of the liquid slug length ahead of the bubble was averaged over the different measurement positions for each flow rate and inclination angle. The results in Fig. 3 show that the maximum normalized approach velocity (at $\ell_s \approx 2D$) decreases with decreasing inclination angle for the same mixture velocity. The onset of acceleration occurs later for a shallow angle as compared to larger inclinations. The data in Fig. 3 for different flow rates collapse on a single curve and approach the value given by (1) at sufficiently large separation distances. The accumulated data were best fitted adopting the curve suggested by Moissis and Griffith (1962) with some modifications:

$$\frac{U_t}{U_{Nick}} = a + b\exp(-c\ell_s/D) + \frac{1}{(\ell_s/D)^d}. \quad (3)$$

The coefficient a represents the normalized elongated bubble translational velocity at large separation distances. The last term, which is absent in the original Moissis and Griffith correlation, is added to account for the slower decay in the translational velocity of elongated bubbles behind relatively long slugs. For additional extensive data on continuous slug flow evolution in vertical and inclined pipes see van Hout et al. (2001, 2002a,b, 2003).

3. Hydrodynamics of the liquid slug—experiments with controlled bubble injection

The results in continuous slug flow clearly indicate that the trailing bubble nose is affected by the velocity

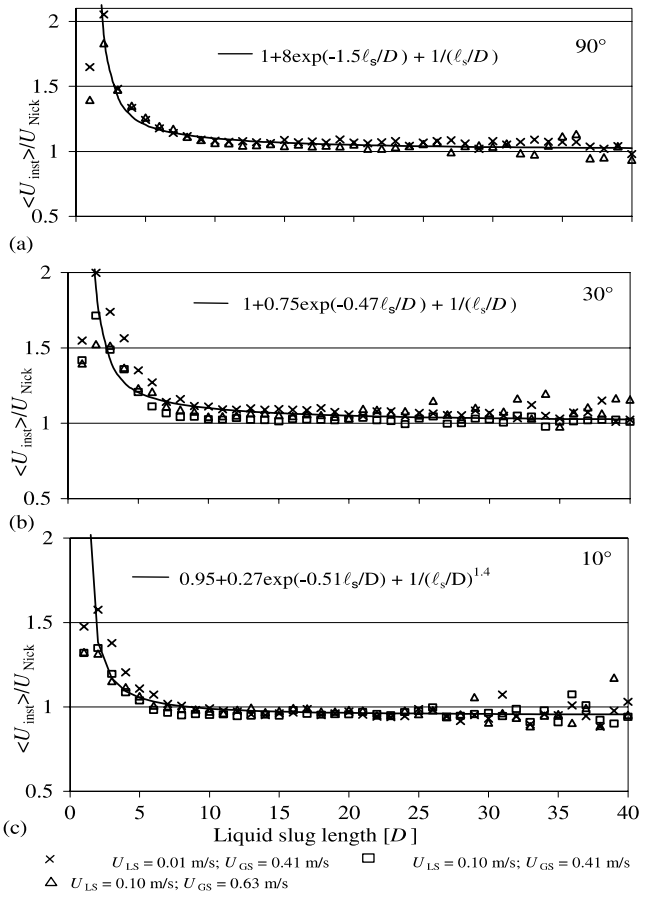

Fig. 3. Averaged instantaneous translational velocity as a function of separation distance for different inclination angles and various flow rates.

field in the liquid phase ahead of it (Shemer and Barnea, 1987; Polonsky et al., 1999b). Information on detailed hydrodynamics in the wake of the leading bubble is therefore indispensable for the understanding of the trailing bubble movement. Measurements of flow field parameters around elongated bubbles in pipes are sparse. Some of them were carried out in continuous slug flow, but more often individual bubbles were injected into pipes to take advantage of controlled experimental conditions.

The length of the wake region increases with increasing Reynolds number based on the mixture velocity. Nakoryakov et al. (1986, 1989) and Kashinsky et al. (2001) investigated the velocity field in vertical upward continuous slug flow using an electrochemical method. Both velocity and wall shear stress measurements were carried out. The Taylor bubble wake length was found to be about 2*D* for all liquid flow rates. The axial centerline velocity in the liquid slug exhibited a maximum at approximately 1*D* from the bubble tail. Intensive turbulent fluctuations were observed in the region where the annular jet mixes with the flow in the wake. Shemer and Barnea (1987) applied a hydrogen bubble technique to visualize the instantaneous velocity profile behind an elongated bubble moving in 20 mm ID vertical and horizontal glass tubes in co-current flowing water. The observed velocity profile was highly distorted in the near wake of the bubble; the profile appeared to be fully developed at about 12*D* from the bubble tail. Ahmad et al. (1998) applied a photochromic dye activation technique to measure the instantaneous velocity profiles in the near wall region around individual and coalescing pairs of Taylor bubbles. Recent results obtained in experiments with controlled bubble injection in our laboratory are presented in the sequel.

3.1. Experimental set-up and data processing

Experiments were carried out in a 4 m long Perspex pipe with ID of 0.025 m. To reduce image distortion, at the measuring station (about 2.5 m from the inlet), a water-filled rectangular transparent box was attached to the pipe. Water in the pipe can be circulated in a closed loop. Bubbles are injected from an air chamber, connected to the test pipe by a computer-controlled injection valve, thus producing Taylor bubbles of any desired length. The digital image processing is employed for the measurements of the instantaneous and time-averaged parameters of the bubble moving along the pipe, such as its propagation velocity and shape, while the particle image velocimetry (PIV) technique provides the flow field in the liquid surrounding the bubble. Two synchronized video cameras are used for the measurements of the bubble propagation velocity along the pipe. In these measurements, illumination is provided by a set of 500 W halogen lamps. In the measurements of the bubble shape, 5 W argon ion laser light sheet about 50 mm high and 1 mm thick was used. For PIV measurements, a pulsed Nd:YAG laser was used as the illumination source and a small amount of almost neutrally buoyant polystirol fluorescent particles, 20–40 μm in diameter, was added to the water. A KODAK ES 1.0 CCD camera with resolution of 1008 by 1018 pixels was operated in triggered double exposure mode that allowed capturing of a pair of two single pulsed frames at a short time interval at a desired frequency. More details on the experiments are given in Polonsky et al. (1999a) and van Hout et al. (2002a).

3.2. Taylor bubble translational velocity and the velocity field ahead of it

In Fig. 4 the vector plot of the PIV-derived mean velocity field in front of a Taylor bubble rising in stagnant water is shown. The spatial resolution in the plot is reduced for better visibility. The effect of the Taylor bubble movement is negligible beyond a distance of about 0.5*D* ahead of its nose. However, small expansion-induced velocities upstream of the bubble nose of

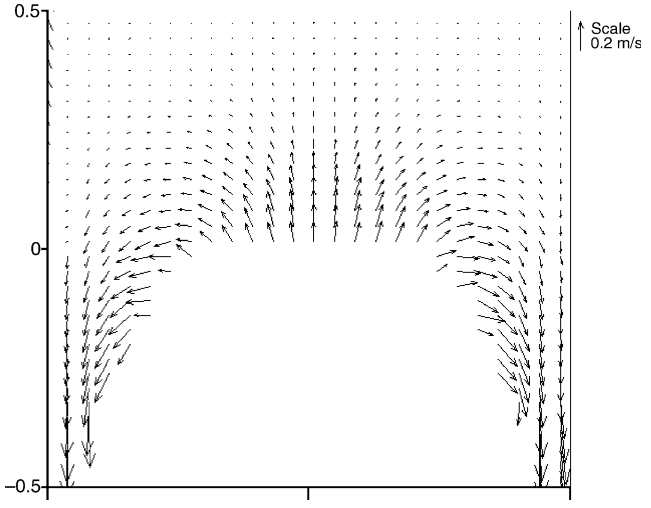

Fig. 4. Velocity vector field in front of a Taylor bubble.

the order of 1.5 mm/s were detected. Upon approaching the bubble nose, the axial centerline velocity increases and flow reversal occurs near the pipe wall at approximately $0.5D$ from the bubble tip. This agrees with Polonsky et al. (1999b).

The translational velocity of the Taylor bubble U_t was calculated from the measured displacement of the bubble nose. The value of the Taylor bubble drift velocity in our facility was found to be $U_d = 17.4$ cm/s, in agreement with Dumitrescu (1943). Substituting (for a single injected bubble) the liquid velocity U_L instead of U_m into (1) allows one to calculate the coefficient C from the measured values of the bubble translational velocity U_t and of U_d. Liquid velocities in the range $-0.14 < U_L < 0.255$ m/s were studied (minus denotes downward flow). The maximum value of the Reynolds number based on the liquid velocity, $Re_L = U_L D/\nu_L$, is thus 6380. The dependence of the coefficient C on U_L as obtained in the present measurements is shown in Fig. 5. For upward flow, the coefficient C decreases from about 2 at very low liquid flow rates, to about 1.2 for the highest flow rates. For stagnant water, the substitution of the gas expansion induced velocity into (1) yields $C \approx 1.5$.

To verify the hypothesis that the value of C in (1) is determined by the maximum liquid velocity ahead of the bubble, the ratio of the maximum to the average velocity determined from the PIV-measured velocity profiles is also shown in Fig. 5. For up-flowing liquid, the values of the ratio of the maximum and the mean velocity in the cross-section, as well as those of C, are lower than 2 and decrease with U_L. This is due to the fact that the entrance length increases with Re_L, and thus at the measurement location the profiles for higher flow rates are less developed. For low values of Re_L, and thus short entrance regions, the value of C in (1) indeed approaches 2. For the stagnant liquid, the mean value of C is close to 1.5, as calculated from the translational velocity data. For interpretation of data for downward flow see Polonsky et al. (1999b).

3.3. Movement of the Taylor bubble bottom

The bottom of a single injected bubble, in contrast to the bubble nose, does not retain a permanent shape while moving along the pipe. As becomes apparent from Fig. 6, these variations in the instantaneous bubble bottom shape become more pronounced with increasing the bubble length, L. For longer bubbles, the sloshing anti-symmetric nature of the bubble bottom oscillation can clearly be observed in the experimental facility even by naked eye. The quasi-periodic character of these oscillations is evident in Fig. 6.

This well-organized pattern suggests the application of the Fourier analysis for a quantitative description. The bubble remains in the camera field of view for more than 2 s for the stagnant liquid experiments, so that the frequency resolution is better than about 0.5 Hz. Power spectra of the bubble tail oscillations in stagnant liquid are presented in Fig. 7. The spectra presented here are averaged over few radial positions for each bubble, and

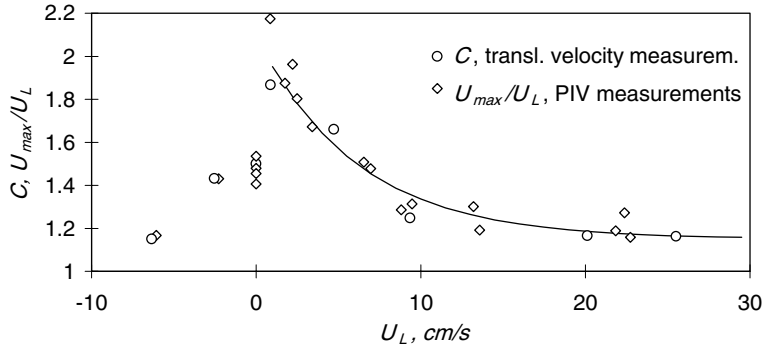

Fig. 5. The relation between C and the velocity profiles ahead of the bubble.

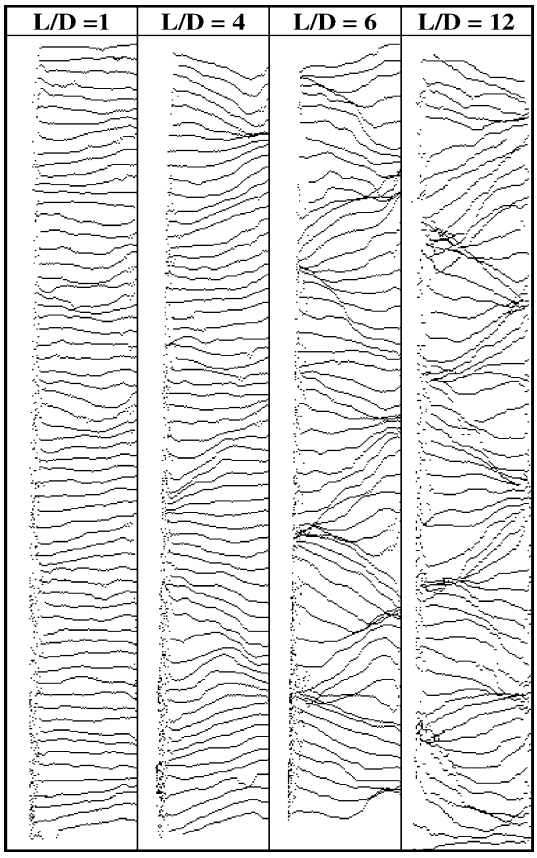

Fig. 6. The consecutive positions of the bubble bottom for different bubble lengths.

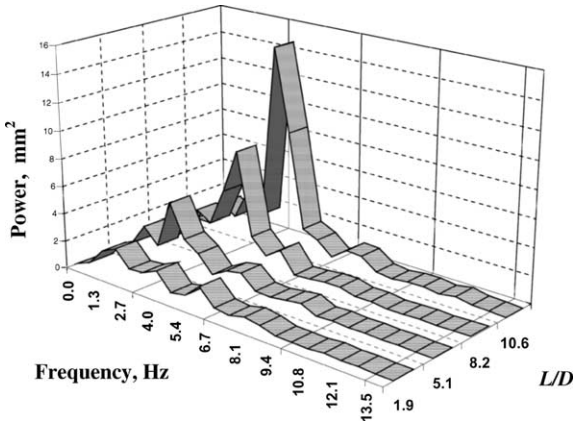

Fig. 7. Spectra of the bubble bottom oscillations.

then for a number of bubbles of similar length. The resonant character of the spectra is clearly seen, and the dominant frequency, about 4 Hz, can be easily identified. The amplitude of the bubble oscillations is apparently growing with the bubble length, while the dependence of the frequency of those oscillations on the bubble length is less pronounced. Additional details on the movement of a single bubble in a vertical pipe can be found in Polonsky et al. (1999a).

3.4. The wake region of the Taylor bubble

The instantaneous velocity field measurements in the Taylor bubble wake region were carried out using PIV. For each set of experimental conditions, 100 Taylor bubbles were injected into the pipe filled with water. The vector plot of the ensemble-averaged velocity field of a Taylor bubble rising in stagnant water is show in Fig. 8a for the bottom area of the falling liquid film and in Fig. 8b for the wake region. The liquid film is accelerated along the bubble as its thickness diminishes. The falling film velocity does not reach its terminal value due to the relatively short bubble length. The film enters the liquid slug as an annular jet creating a toroidal vortex stretching up to $2D$ in the near wake of the Taylor bubble. A much weaker vortex with an opposite sense of rotation can be observed in Fig. 8b between the axial distances $2 < x/D < 4$. As expected, the mean velocity field exhibits axial symmetry.

The variation of the ensemble-averaged axial velocity at the pipe centerline is shown in Fig. 9 as a function of the distance from the bubble. Note that at the bubble interface, the axial velocity component in the liquid in front and behind the bubble is equal to the bubble velocity. The velocity in front of the bubble decreases fast and vanishes at $x/D > 0.5$, with the exception of the expansion-induced velocities (cf. Fig. 4). In contrast to the monotonous decrease in front of the bubble, the centerline axial velocity in the bubble wake increases initially to about 0.6 m/s at $x/D \approx 1$, then decreases fast, crosses the x-axis at $x/D = 2$ and becomes negative (downward direction) with a maximum absolute value of about 0.05 m/s at $x/D \approx 2.5$. These single-bubble results in stagnant liquid are in general agreement with the experiments of Nakoryakov et al. (1986, 1989) in continuous slug flow. For $x/D > 5$ the axial velocity at the centerline becomes positive again, attains a local maximum at about $x/D = 6$ and then slowly decreases to zero at larger distances from the bubble. The change of sign of the mean axial velocity at the centerline reflects the sequence of vortex rings with opposite sense of rotation as seen in Fig. 8.

The mean velocities in the wake of the Taylor bubble decay fast and effectively vanish at a relatively short distance from the bubble tail. The instantaneous velocities, however, remain noticeable even at large distances behind the bubble. It is commonly speculated that the tip location and the translational velocity of the elongated bubble in slug flow are affected by the local instantaneous maximum velocity $U_{\max}$ in the liquid slug just ahead of the bubble. It is therefore instructive to examine the variation of $U_{\max}$ as a function of the distance x/D from the bubble bottom. For each injected bubble and axial cross-section x/D, the local instantaneous $U_{\max}$ was determined. These values were then averaged over the whole ensemble (100 bubbles).

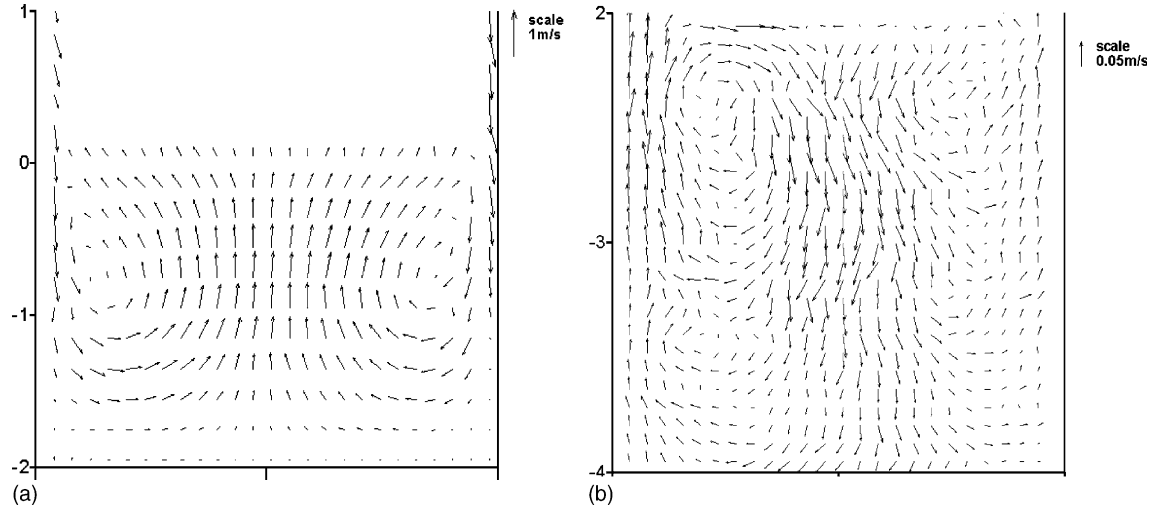

Fig. 8. Ensemble-averages velocity plots behind the Taylor bubble: (a) in the liquid film and in the near wake region and (b) at the average distance of $3D$ from the bubble bottom.

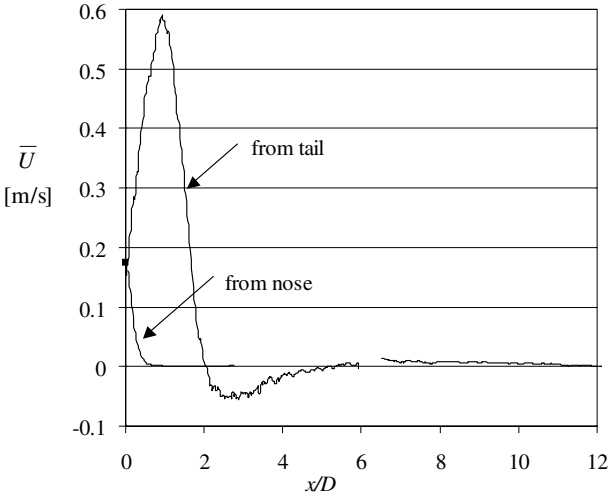

Fig. 9. The variation of the ensemble averaged axial velocity at the centerline of the pipe as a function of the distance from the Taylor bubble nose and tail.

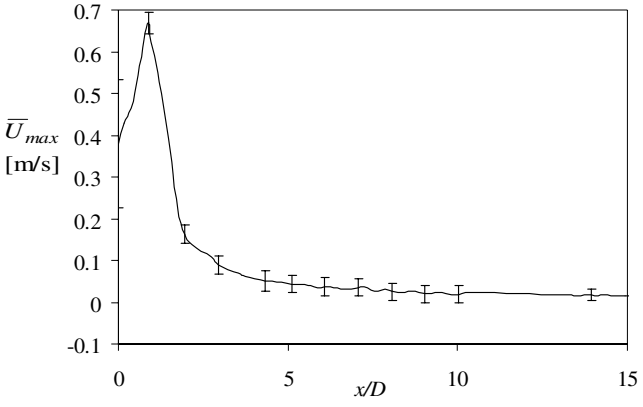

Fig. 10. Ensemble-averaged instantaneous maximum velocities in the cross-section vs. the distance.

The resulting variation of $\overline{U}_{\max}$ with x/D is presented in Fig. 10. The error bars are also given in this figure. Note that in contrast to the mean axial velocities at the centerline that essentially vanish at $x/D = 12$, see Fig. 9, velocities $\overline{U}_{\max}$ at this location retain values of a few cm/s and decay much slower. Even at x/D approaching 50 the maximum velocities are only slightly below 0.5 cm/s. This fact can account for the non-zero relative approach velocities of the trailing bubble at considerable distances from the leading one as observed by Aladjem Talvy et al. (2000). Moreover, in the region $2 < x/D < 5$, where the average centerline velocity is directed downwards (Fig. 9), the maximum instantaneous velocities, mostly located close to pipe walls, are positive and have relatively high values comparable with the Taylor bubble drift velocity U_{d}.

3.5. Two consecutive elongated bubbles

The motion of the trailing bubble is strongly affected by the wake of the leading Taylor bubble, cf. Fig. 1. The trailing bubble's nose is deformed and its shape changes rapidly in the course of the bubble approach (Aladjem Talvy et al., 2000). Shemer and Barnea (1987) and Polonsky et al. (1999b) suggested that trailing bubble tip follows the location of the maximum liquid velocity in the profile ahead of the bubble.

The temporal variation of the instantaneous radial position of the tip of the trailing bubble nose is plotted in Fig. 11. The increase in the amplitude of the nose tip oscillations with decreasing distance between the bubbles is clearly seen. The characteristic frequency of the quasi-periodic nose tip oscillations is close to the peak

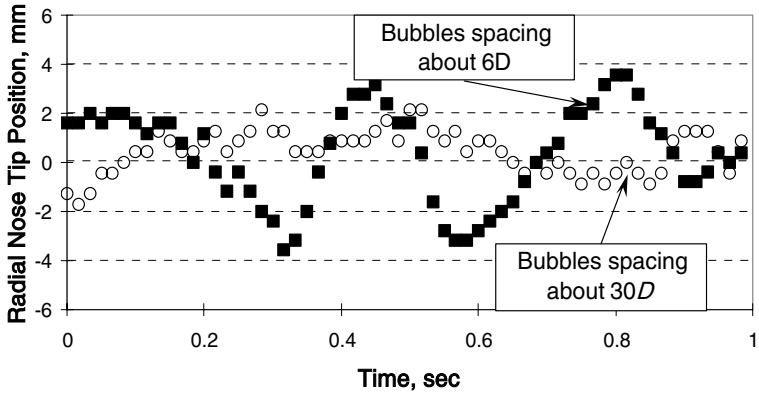

Fig. 11. Radial oscillations of the trailing bubble tip at two distances from the leading Taylor bubble.

frequency in the leading bubble bottom oscillations in Fig. 7. This suggests that the instantaneous rate of trailing bubble propagation is controlled to a certain extent by the quasi-periodic oscillations of the bottom of the leading bubble and the velocity field induced in the leading bubble wake by those oscillations.

The fluctuations of the liquid velocity ahead of the trailing bubble can either accelerate the bubble propagation or slow it down, depending on the instantaneous location of the bubble tip and the sign of the fluctuation of the axial velocity. The intensity of these fluctuations varies significantly with the distance from the leading bubble bottom. The oscillations of the trailing bubble velocity therefore become more violent as the trailing Taylor bubble approaches the leading one.

In Fig. 12, histograms representing the frequencies of appearance of the instantaneous approach velocities of $6D$ long bubbles are given for three ranges of the bubble spacing. For each bubble spacing range, the ensemble size is about 1000. As the distance between the bubbles decreases, the distributions slide to the right, in the direction of higher trailing bubble propagating velocities, and the dispersion of the data becomes wider.

Fig. 12 further supports the observation that interaction between bubbles apparently exists at distances exceeding what was previously considered to be "a sta-

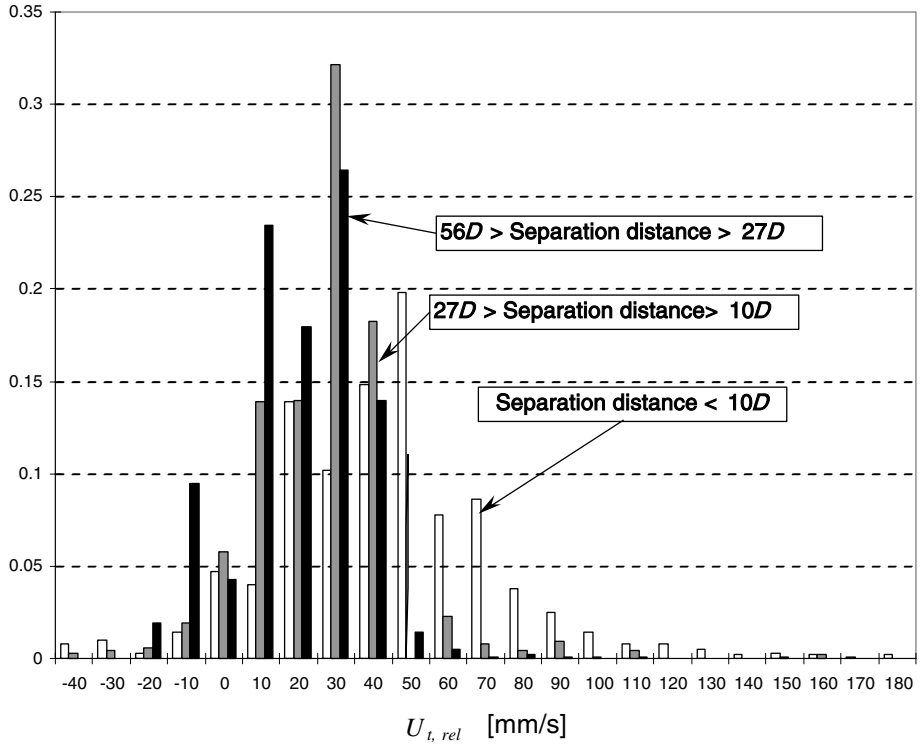

Fig. 12. Histograms of the instantaneous relative velocity of the trailing bubble at various separation distances.

ble liquid slug length''. In vertical slug flow, the stable liquid slug length is assumed to be around $16D$ (Moissis and Griffith, 1962), yet, the experimental results in Fig. 12 indicate an average positive rate of approach for much larger spacing between bubbles. Pinto et al. (2001) recently reported that the interaction between bubbles is restricted to quite short distances, but this conjecture may stem from insufficient accuracy of their experiments.

4. Concluding remarks

Some results of an extensive research program on investigation of statistics and hydrodynamics of slug flow are reported here. The research is carried out in two directions. First, detailed statistics of numerous parameters representing continuous slug flow is investigated in pipes of two different diameters. Due to space limitations, only some representative results are given here. Comprehensive report on these studies can be found in van Hout et al. (2001, 2002a,b). The obtained results corroborate the well-known understanding that successful modeling of slug flow that will enable prediction of the essential hydrodynamic and heat transfer parameters, requires detailed experimental data as an input. The complexity of slug flow regime thus suggested the second research direction, i.e. experiments with individual bubbles injected into pipes with stagnant or flowing liquid. Motivation for this approach comes from realization of the fact that the movement of an elongated bubble in continuous slug flow is determined by the velocity field in the liquid ahead of it. For given flow conditions, this velocity field is mainly determined by the movement of the preceding elongated bubble. The main advantage of individual bubble injection is in possibility to apply advanced optical experimental methods, like digital image processing and PIV. Although these methods can be applied to some extent in continuous slug flow experiments (see e.g. van Hout et al., 2002b), much more detailed measurements can be carried out for the ''clean'' conditions of controlled bubble injection.

In particular, the movement of a single bubble in a vertical pipe was studied in detail (Polonsky et al., 1999a,b). Strong turbulence generated when the annular fast liquid film mixes with the upward flowing liquid behind the Taylor bubble is dominant in the near wake region, resulting in an asymmetric instantaneous velocity field characterized by small-scale vortices and high local velocities. In the far field ($x/D > 25$), only vortices of the scale of the pipe diameter survive and the separation distance between the consecutive vortices may be related to the characteristic frequency of the bubble bottom oscillations (van Hout et al., 2001). Accurate measurements of the instantaneous velocity of the trailing bubble performed by Aladjem Talvy et al. (2000) allowed suggesting empirical correlation between the bubble velocity and the liquid slug length ahead of it. When these results were used as an input to Barnea and Taitel (1993) predictive model, reasonable agreement with experiments was obtained in vertical and inclined continuous slug flow (van Hout et al., 2001, 2003).

Extensive further work in this field is required. Modeling of slug flow should include the understanding of the statistics of the governing hydrodynamic parameters and nor just their mean values. Additional experiments are planned to accumulate the necessary data on a single elongated bubble movement for a wide range of operational parameters, including the Reynolds number and pipe inclination. In-depth study of the interaction of two consecutive bubbles is necessary. To understand the quite complicated motion of the trailing bubble in the wake of the leading one, detailed measurements of the flow velocity in the liquid slug are to be carried out simultaneously with the measurements of the trailing bubble movement.

Acknowledgements

This work was supported by a grant from the Israel Science Foundation. The research was conducted in collaboration with D. Barnea, S. Polonsky, C. Aladjem Talvy, R. van Hout and A. Goulitski.

References

Ahmad, W.R., DeJesus, J.M., Kawaji, M., 1998. Falling film hydrodynamics in slug flow. Chem. Eng. Sci. 53, 123–130.

Aladjem Talvy, C., Shemer, L., Barnea, D., 2000. On the interaction between two consecutive elongated bubbles in a vertical pipe. Int. J. Multiphase Flow 26, 1905–1923.

Andreussi, P., Bendiksen, K.H., Nydal, O.J., 1993. Void distribution in slug flow. Int. J. Multiphase Flow 19, 817–828.

Barnea, D., Shemer, L., 1989. Void fraction measurement in vertical slug flow: Applications to slug characteristics and transitions. Int. J. Multiphase Flow 15, 495–504.

Barnea, D., Taitel, Y., 1993. A model for slug length distribution in gas–liquid slug flow. Int. J. Multiphase Flow 19, 829–838.

Bendiksen, K.H., 1984. An experimental investigation of the motion of long bubbles in inclined tubes. Int. J. Multiphase Flow 10, 467–483.

Benjamin, T.B., 1968. Gravity currents and related phenomena. J. Fluid Mech. 31, 209–248.

Bernicot, M., Drouffe, J.M., 1989. Slug length distribution in two-phase transportation systems. In: Proceedings of the 4th International Conference on Multi-Phase Flow, BHRA. pp. 485–493.

Cook, M., Behnia, M., 2001. Slug length prediction in near horizontal gas–liquid intermittent flow. Chem. Eng. Sci. 55, 2009–2018.

Costigan, G., Whalley, P.B., 1997. Slug flow regime identification from dynamic void fraction measurements in vertical air–water flows. Int. J. Multiphase Flow 23, 263–282.

Dhulesia, H., Bernicot, M., Deheuvels, P., 1991. Statistical analysis and modelling of slug lengths. In: Proceedings of the 5th International Conference on Multi-Phase Production, BHRA. pp. 80–112.

Dumitrescu, D.T., 1943. Strömung an einer Luftblase im senkrechten Rohr. Z. Ang. Math. Mech. 23, 139–149.

Fabre, J., Liné, A., 1992. Modeling of two-phase flow. Ann. Rev. Fluid Mech. 24, 21–46.

Felizola, H., Shoham, O., 1995. A unified model for slug flow in upward inclined pipes. J. Energy Res. Technol. 117, 7–12.

Griffith, P., Wallis, G.B., 1961. Two-phase flow. J. Heat Transfer 83, 307–320.

Kashinsky, O.N., Gorelik, R.S., Randin, V.V., 2001. Structure of upward slug flow in a vertical pipe. In: Proceedings of the 5th World Conference on Experimental Heat Transfer, Fluid Mechanics and Thermodynamics 2, 1472–1475.

Moissis, R., Griffith, P., 1962. Entrance effects in a two-phase slug flow. J. Heat Transfer 84, 366–370.

Nakoryakov, V.E., Kashinski, O.N., Kozmenko, B.K., 1986. Experimental study of gas–liquid slug flow in a small-diameter vertical pipe. Int. J. Multiphase Flow 12, 337–355.

Nakoryakov, V.E., Kashinski, O.N., Petukhov, A.V., Gorelik, R.S., 1989. Study of local hydrodynamic scharacteristics of upward slug flow. Exp. Fluids 7, 560–566.

Nicklin, D.J., Wilkes, J.O., Davidson, J.F., 1962. Two-phase flow in vertical tubes. Trans. Inst. Chem. Engrs. 40, 61–68.

Nydal, O.J., Pintus, S., Andreussi, P., 1992. Statistical characterization of slug flow in horizontal pipes. Int. J. Multiphase Flow 18, 439–453.

Pinto, A.M.F.R., Pinheiro, M.N., Campos, J.B.L.M., 1998. Coalescence of two gas slugs rising in a co-current flowing liquid in vertical tubes. Chem. Eng. Sci. 53, 2973–2983.

Pinto, A.M.F.R., Pinheiro, M.N., Campos, J.B.L., 2001. On the interaction of Taylor bubbles rising in two-phase co-current slug flow in vertical columns: turbulent wakes. Exp. Fluids 31, 643–652.

Polonsky, S., Barnea, D., Shemer, L., 1999a. Averaged and time-dependent characteristics of the motion of an elongated bubble in a vertical pipe. Int. J. Multiphase Flow 25, 795–812.

Polonsky, S., Shemer, L., Barnea, D., 1999b. The relation between the Taylor bubble motion and the velocity field ahead of it. Int. J. Multiphase Flow 25, 957–975.

Shemer, L., Barnea, D., 1987. Visualization of the instantaneous velocity profiles in gas–liquid slug flow. PhysicoChem. Hydrodyn. 8, 243–253.

Shoham, O., Dukler, A.E., Taitel, Y., 1982. Heat transfer during intermittent-slug flow in horizontal tubes. Ind. Eng. Chem. Fundam. 21, 312–319.

van Hout, R., Shemer, L., Barnea, D., 1992. Spatial distribution of void fraction within the liquid slug and some other related slug parameters. Int. J. Multiphase Flow 18, 831–845.

van Hout, R., Barnea, D., Shemer, L., 2001. Evolution of statistical parameters of gas–liquid slug flow along vertical pipes. Int. J. Multiphase Flow 27, 1579–1602.

van Hout, R., Gulitski, A., Barnea, D., Shemer, L., 2002a. Experimental investigation of the velocity field induced by a Taylor bubble rising in stagnant water. Int. J. Multiphase Flow 28, 579–596.

van Hout, R., Barnea, D., Shemer, L., 2002b. Translational velocities of elongated bubbles in continuous slug flow. Int. J. Multiphase Flow 28, 1333–1350.

van Hout, R., Shemer, L., Barnea, D., 2003. Evolution of hydrodynamic and statistical parameters of gas–liquid slug flow along inclined pipes. Chem. Eng. Sci. 58, 115–133.

Zukoski, E.E., 1966. Influence of viscosity, surface tension, and inclination angle on the motion of long bubbles in closed tubes. J. Fluid Mech. 25, 821–837.